

# Mechanical properties of the radio frequency field emitted by an antenna array

H. Then<sup>1,\*</sup> and B. Thidé<sup>2,†</sup>

<sup>1</sup>*Institute of Physics, Carl von Ossietzky Universität Oldenburg, D-26111 Oldenburg, Germany*

<sup>2</sup>*Swedish Institute of Space Physics, Ångström Laboratory, P. O. Box 537, SE-751 21 Uppsala, Sweden*

Angular momentum densities of electromagnetic beams are connected to helicity (circular polarization) and topological charge (azimuthal phase shift and vorticity). Computing the electromagnetic fields emitted by a circular antenna array, analytic expressions are found for the densities of energy, linear and angular momentum in terms of helicity and vorticity. It is found that the angular momentum density can be separated into spin and orbital parts, a result that is known to be true in a beam geometry. The results are of importance for information-rich radio astronomy and space physics as well as novel radio, radar, and wireless communication concepts.

PACS numbers: 03.50.De,42.50.Tx,41.20.Jb,07.57.-c

Keywords: classical electromagnetism, optical angular momentum, electromagnetic wave propagation, radio-wave instruments

## I. INTRODUCTION

As Maxwell showed, any interaction between electromagnetic (em) radiation and matter is inevitably accompanied by an exchange of momentum. In addition to linear momentum, Poynting [1] inferred from a mechanical analogy that circularly polarized light must carry spin angular momentum and Allen et al. [2] argued that Laguerre-Gaussian laser modes must carry orbital angular momentum. The exchange of spin angular momentum between radiation and a mechanical body was demonstrated experimentally by Beth in 1935 [3], while the transfer of em orbital angular momentum to mechanical orbital angular momentum of particles was experimentally demonstrated only recently [4, 5, 6].

During the past decade the application of em spin and orbital angular momentum has come to the fore in optics [7] and in atomic and molecular physics [8]. The orbital angular momentum of electromagnetic beams now takes an important position in various fields of research and applications, ranging from manipulating and orienting small particles [9], astronomy and astrophysics [10, 11, 12, 13], novel wireless communication concepts [14, 15], quantum entanglement [16], cryptography, and quantum computation [17]. Applications for the use of the orbital angular momentum in the radio domain, allowing digital manipulation under software control, were proposed in Ref. 18, including radio astronomy and space physics [19, 20, 21, 22, 23, 24, 25, 26, 27, 28, 29].

In the literature, different views can be found concerning the possibility of separating the spin and orbital angular momentum; see Refs. 30, 31, 32, 33. In computing the electromagnetic beams emitted by a circular antenna array, and expressing the angular momentum density explicitly in terms of helicity and vorticity, the present paper shows that the angular momentum of the emitted beams can be clearly separated into parts that belong to helicity and vorticity, respectively. The separation is associated with the separation of an-

gular momentum into spin and orbital parts, a result that has been previously shown for optical beams [30, 34]. Crucial for the analytic computation is the fact that the radiated densities of energy, linear momentum, and angular momentum are homogeneous functions of distance. This allows to neglect certain terms in the expressions for these quantities. Since helicity and vorticity are uniquely linked to the phases of the transverse field components, it is possible to emit and detect em beams with spin and orbital angular momentum via transverse field triangulation, dealing solely with first order quantities which can easily be utilized without the need to measure weak longitudinal components.

In order to simplify the present analysis, an approximation is made in the geometrical setup by assuming an array with a continuum of infinitely many elemental antennas [35].

## II. SETUP

The vector potential of a single or crossed electric dipole antenna that is in harmonic oscillation with frequency  $\omega$  can be expressed as

$$\mathbf{A}(\mathbf{r}, t) = -\frac{\mu_0 d}{8\pi} \mathbf{J}(t) \frac{e^{ikr}}{r}, \quad (1)$$

cf. Eqs. (9.16) and (9.27) in [36]. Here  $i$  is the imaginary unit,  $k$  is the magnitude of the wave vector,  $\hat{\mathbf{f}}$  is the unit vector in the direction of  $\mathbf{r}$ ,  $\mu_0$  is the magnetic permeability,  $d$  is the length of each dipole antenna, and  $\mathbf{J}$  is the antenna current.

Taking the potentials and fields to be complex valued, the harmonic time dependence is attributed by multiplying a stationary antenna current  $\mathbf{I}$  with the appropriate complex factor,

$$\mathbf{J}(t) = \mathbf{I} e^{-i\omega t}. \quad (2)$$

The physical fields result from taking the real parts.

Placing  $N$  crossed dipole antennas on a circle at the positions

$$\mathbf{r}_n = \begin{pmatrix} R \cos(2\pi n/N) \\ R \sin(2\pi n/N) \\ 0 \end{pmatrix}, \quad n = 1 \dots N, \quad (3)$$

\*Electronic address: holger.then@uni-oldenburg.de

†Also at LOIS Space Centre, Växjö University, SE-351 95 Växjö, Sweden; Electronic address: bt@ifu.se

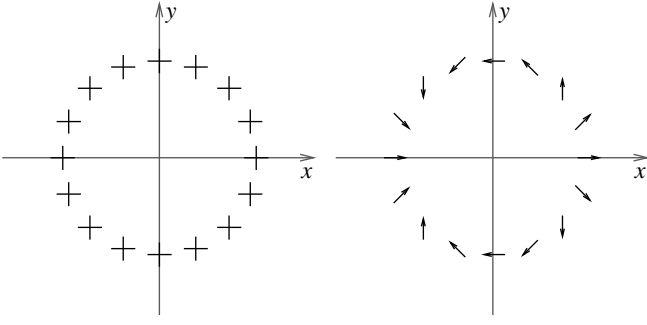


FIG. 1: Plots of the  $N$  crossed dipole antennas and their currents. The left panel displays the positions and orientations of the crossed dipole antennas, and the right panel displays the current vector at each crossed dipole for  $N = 16$ ,  $h = 1$ ,  $l = -2$ , and  $t = 0$ .

where  $R$  is the radius of the antenna array [see Fig. 1 (left)], and feeding the  $n$ th antenna element with the current

$$\mathbf{I}_n = \frac{1}{\sqrt{2}} \begin{pmatrix} I \\ ihI \\ 0 \end{pmatrix} e^{2\pi iln/N}, \quad n = 1 \dots N, \quad (4)$$

[see Fig. 1 (right)], the total vector potential reads

$$\mathbf{A} = \frac{1}{\sqrt{2}} \begin{pmatrix} 1 \\ ih \\ 0 \end{pmatrix} \mathcal{A}(r) \mathcal{C}(\theta, \phi) \quad (5)$$

with

$$\mathcal{A} = -\frac{I\mu_0 d}{8\pi} \frac{e^{ikr}}{r} \quad (6)$$

and

$$\mathcal{C} = \sum_{n=1}^N e^{2\pi iln/N} e^{-ik\hat{\mathbf{r}} \cdot \mathbf{r}_n}, \quad (7)$$

where  $I$  is the amplitude of the antenna currents,  $h = \pm 1$  is the helicity associated with circular polarization, and  $l \in \mathbb{Z}$  is the topological charge. The topological charge attributes an azimuthal phase shift of  $\exp(2\pi iln/N)$  to the antenna currents and is associated with vorticity.

If the number of antennas  $N$  is sufficiently large (typically  $N \geq 16$ ), the sum in  $\mathcal{C}$  can be approximated by a Riemann integral and expressed by its residue in the complex  $\zeta$  plane,

$$\mathcal{C}(\theta, \phi) \simeq \frac{N}{2\pi} \int_0^{2\pi} d\Phi e^{il\Phi} e^{-ikR \sin \theta \cos(\Phi - \phi)} \quad (8)$$

$$= e^{il\phi} N \operatorname{Res}_{\zeta=0} \frac{1}{l} e^{-ikR \sin \theta \cosh(\frac{1}{l} \ln \zeta)}, \quad (9)$$

yielding

$$\frac{\partial}{\partial \phi} \ln \mathcal{C} = il \quad (10)$$

and

$$\frac{\partial}{\partial \theta} \ln \mathcal{C} = \text{real} \quad (11)$$

which implies that  $\mathcal{C}^* \mathcal{C}$  is independent of  $\phi$ .

### III. FIELDS

From the vector potential follows the magnetic field

$$\mathbf{B} = \nabla \times \mathbf{A}. \quad (12)$$

Separating the magnetic field into its far and its near field terms,

$$\mathbf{B} = \mathbf{B}_{\text{far}} + \mathbf{B}_{\text{near}}, \quad (13)$$

results in

$$\mathbf{B}_{\text{far}} = ik\hat{\mathbf{r}} \times \mathbf{A} \quad (14)$$

and

$$\mathbf{B}_{\text{near}} = e^{ikr} \nabla \times (\mathbf{A} e^{-ikr}), \quad (15)$$

where  $e^{-ikr} \mathbf{B}_{\text{far}}$  and  $e^{-ikr} \mathbf{B}_{\text{near}}$  are homogeneous functions in  $r$  of degree  $-1$  and  $-2$ , respectively.

The electric field outside the sources is given by

$$\mathbf{E} = \frac{ic}{k} \nabla \times \mathbf{B}, \quad (16)$$

where  $c$  is the speed of light. The electric field results in

$$\mathbf{E} = \mathbf{E}_{\text{far}} + \mathbf{E}_{\text{inter}} + \mathbf{E}_{\text{near}} \quad (17)$$

with

$$\mathbf{E}_{\text{far}} = ikc[\mathbf{A} - (\hat{\mathbf{r}} \cdot \mathbf{A})\hat{\mathbf{r}}], \quad (18)$$

$$\mathbf{E}_{\text{inter}} = -c[\hat{\mathbf{r}}(\nabla \cdot (\mathbf{A} e^{-ikr})) + \nabla(\hat{\mathbf{r}} \cdot \mathbf{A} e^{-ikr})] e^{ikr}, \quad (19)$$

and

$$\mathbf{E}_{\text{near}} = \frac{ic}{k} [\nabla(\nabla \cdot (\mathbf{A} e^{-ikr})) - \nabla^2(\mathbf{A} e^{-ikr})] e^{ikr}. \quad (20)$$

The individual terms of the electric field are called the far,  $\mathbf{E}_{\text{far}}$ , the intermediate,  $\mathbf{E}_{\text{inter}}$ , and the near electric field,  $\mathbf{E}_{\text{near}}$ . Apart from the complex phase, they are homogeneous functions in  $r$  of degree  $-1$ ,  $-2$ , and  $-3$ , respectively.

### IV. DENSITIES OF ENERGY AND MOMENTA

Imagine a set of concentric spheres centered on the radiation source at the origin. If a physical quantity  $Q$  is conserved, the total flow of  $Q$  through the sphere surfaces must be the same for each sphere. This is only possible if the  $r^2$  dependence of the surface area cancels with an  $r^{-2}$  dependence of the density of the conserved quantity. Hence, the density of any conserved quantity  $Q$  that propagates radially with a constant speed is required to be homogeneous in  $r$  of degree  $-2$ .

The em field energy density is defined by

$$u = \frac{\epsilon_0}{4} (\mathbf{E} \cdot \mathbf{E}^* + c^2 \mathbf{B} \cdot \mathbf{B}^*), \quad (21)$$

where  $\epsilon_0$  is the electric permittivity of free space. The conservation law of energy imposes the condition that the radiated energy density must be homogeneous in  $r$  of degree  $-2$ . This condition is fulfilled by the leading order term of the energy density,

$$u_{\text{far}} = \frac{\epsilon_0}{4} (\mathbf{E}_{\text{far}} \cdot \mathbf{E}_{\text{far}}^* + c^2 \mathbf{B}_{\text{far}} \cdot \mathbf{B}_{\text{far}}^*). \quad (22)$$

The linear momentum density is given by the Poynting vector

$$\mathbf{p} = \frac{\epsilon_0}{2} \Re[\mathbf{E} \times \mathbf{B}^*], \quad (23)$$

which can be split into homogeneous functions in  $r$  of degree  $-2$ ,  $-3$ , and higher order terms,

$$\mathbf{p} = \mathbf{p}_{\text{far}} + \mathbf{p}_{\text{next}} + \mathbf{p}_{\text{rest}} \quad (24)$$

with

$$\mathbf{p}_{\text{far}} = \frac{\epsilon_0}{2} \Re[\mathbf{E}_{\text{far}} \times \mathbf{B}_{\text{far}}^*], \quad (25)$$

$$\mathbf{p}_{\text{next}} = \frac{\epsilon_0}{2} \Re[\mathbf{E}_{\text{far}} \times \mathbf{B}_{\text{near}}^* + \mathbf{E}_{\text{inter}} \times \mathbf{B}_{\text{far}}^*] \quad (26)$$

and

$$\mathbf{p}_{\text{rest}} = O(1/r^4). \quad (27)$$

Due to the conservation of linear momentum, the radiated linear momentum density is given by the far field terms,  $\mathbf{E}_{\text{far}}$  and  $\mathbf{B}_{\text{far}}$ , only.

The angular momentum density is defined by

$$\mathbf{j} = \mathbf{r} \times \mathbf{p}. \quad (28)$$

Because of the conservation law of angular momentum the radiated angular momentum density is homogeneous in  $r$  of degree  $-2$ . This has important consequences. Namely, the pure far field does not contribute to the radiated angular momentum density, since  $\mathbf{r} \times \mathbf{p}_{\text{far}}$  would then be a homogeneous function in  $r$  of degree  $-1$ , but this term vanishes due to the fact that  $\mathbf{p}_{\text{far}}$  is directed along  $\mathbf{r}$ . Instead, it is the next order term,

$$\mathbf{j}_{\text{far}} = \mathbf{r} \times \mathbf{p}_{\text{next}}, \quad (29)$$

that yields the radiated angular momentum density.

Plugging the vector potential expression (5) into the expressions for the magnetic and electric fields and evaluating the radiated densities of energy, linear momentum, and angular momentum results in

$$u_{\text{far}} = \frac{k^2}{4\mu_0} \left( \frac{I\mu_0 d}{8\pi r} \right)^2 (1 + \cos^2 \theta) (\mathcal{E}^* \mathcal{E}), \quad (30)$$

$$\mathbf{p}_{\text{far}} = \frac{\hat{\mathbf{r}} k^2}{4c\mu_0} \left( \frac{I\mu_0 d}{8\pi r} \right)^2 (1 + \cos^2 \theta) (\mathcal{E}^* \mathcal{E}), \quad (31)$$

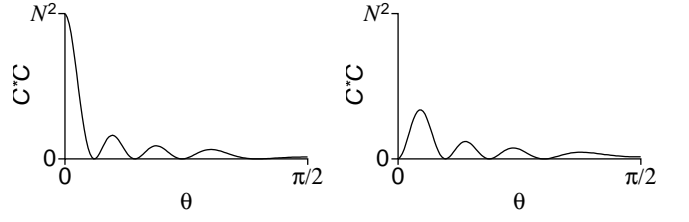


FIG. 2: Plots of the function  $\mathcal{E}^* \mathcal{E}$ . Notice the influence of  $l$  on the graph. Here  $l = 0$  (left) and  $l = \pm 1$  (right).

and

$$\mathbf{j}_{\text{far}} = \frac{-\hat{\boldsymbol{\theta}} k}{4c\mu_0} \left( \frac{I\mu_0 d}{8\pi r} \right)^2 \left\{ h \left( 2 \sin \theta (\mathcal{E}^* \mathcal{E}) - \cos \theta \frac{\partial}{\partial \theta} (\mathcal{E}^* \mathcal{E}) \right) + l \frac{1 + \cos^2 \theta}{\sin \theta} (\mathcal{E}^* \mathcal{E}) \right\}, \quad (32)$$

where  $\hat{\mathbf{r}}$ ,  $\hat{\boldsymbol{\theta}}$ , and  $\hat{\boldsymbol{\phi}}$  are the unit vectors of spherical coordinates. Since the density of angular momentum scales with distance like  $r^{-2}$ , the angular momentum is transported all the way out to infinity, a fact that is not always well appreciated.

## V. SPIN AND ORBITAL ANGULAR MOMENTUM

Separating the angular momentum density in terms that depend on the topological charge  $l$  only and in terms that depend on the helicity  $h$ ,

$$\mathbf{j}_{\text{far}} = \mathbf{l}_{\text{far}} + \mathbf{s}_{\text{far}}, \quad (33)$$

allows to identify the topological charge (vorticity) with the orbital angular momentum density

$$\mathbf{l}_{\text{far}} = l \frac{-\hat{\boldsymbol{\theta}} k^2}{4\omega\mu_0} \left( \frac{I\mu_0 d}{8\pi r} \right)^2 \left( \frac{1 + \cos^2 \theta}{\sin \theta} \right) (\mathcal{E}^* \mathcal{E}), \quad (34)$$

and the helicity (polarization) with the spin orbital angular momentum density

$$\mathbf{s}_{\text{far}} = h \frac{-\hat{\boldsymbol{\theta}} k^2}{4\omega\mu_0} \left( \frac{I\mu_0 d}{8\pi r} \right)^2 \left( 2 \sin \theta (\mathcal{E}^* \mathcal{E}) - \cos \theta \frac{\partial}{\partial \theta} (\mathcal{E}^* \mathcal{E}) \right). \quad (35)$$

Surprisingly, the orbital angular momentum density is easier to describe than the density of the spin angular momentum. The density of the orbital angular momentum is completely independent of the helicity, but the spin angular momentum density depends via  $\mathcal{E}^* \mathcal{E}$  on the topological charge. If the topological charge vanishes,  $\mathcal{E}^* \mathcal{E}$  has its maximum at  $\theta = 0$ , while for any non-vanishing topological charge,  $\mathcal{E}^* \mathcal{E}$  is zero at  $\theta = 0$ ,

$$(\mathcal{E}^* \mathcal{E})|_{\theta=0} = \begin{cases} N^2 & \text{if } l = 0, \\ 0 & \text{if } l \neq 0, \end{cases} \quad (36)$$

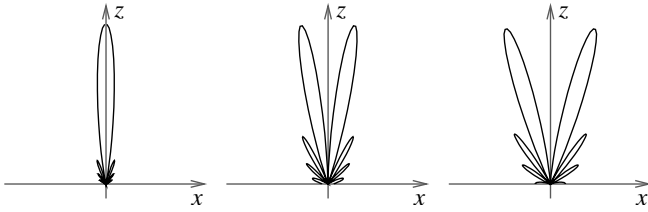


FIG. 3: Radiation patterns of the linear momentum for radio beams generated by a circular antenna array with radius  $2\lambda$ ; all antennas are directly over ground. Without ground the electromagnetic waves would also be emitted symmetrically into the lower half space. The patterns are for  $l = 0$  (left),  $l = \pm 1$  (middle), and  $l = \pm 2$  (right).

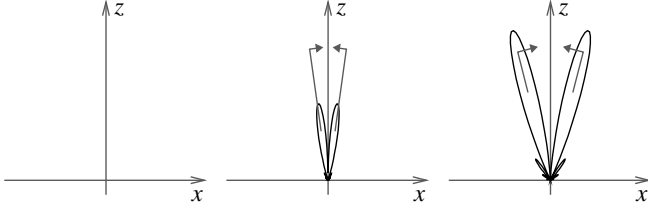


FIG. 4: Radiation patterns for the orbital angular momentum. The direction of the orbital angular momentum density vectors is in the direction of  $-\hat{\theta}l$  as displayed by the arrows  $\hat{r}$  and  $\hat{\imath}$ . The patterns are for  $l = 0$  (left),  $l = 1$  (middle), and  $l = 2$  (right).

and

$$\frac{\partial}{\partial \theta} (\mathcal{E}^* \mathcal{E})|_{\theta=0} = 0. \quad (37)$$

Figure 2 shows graphs of  $\mathcal{E}^* \mathcal{E}$ . For all plots, an array radius of  $R = 2\lambda$  was used, where  $\lambda = 2\pi/k$  is the wavelength.

## VI. RADIATION PATTERNS

Radiation patterns of the energy (linear momentum) are shown in Fig. 3. If the topological charge vanishes, i.e.  $l = 0$ , the particular antenna array chosen here emits a beam that has maximum intensity on the  $z$  axis. If the topological charge is non-vanishing,  $l \neq 0$ , the fields of the beam cancel on the  $z$  axis, resulting in a doughnut shaped beam profile that becomes wider for larger absolute values of the topological charge.

The far-field approximation of the Poynting vector is proportional to the energy density and points from the antenna array radially outward,

$$\mathbf{p}_{\text{far}} = \frac{\hat{\mathbf{r}}}{c} u_{\text{far}}. \quad (38)$$

Therefore, the radiation pattern of the linear momentum is identical to that of the energy.

Radiation patterns of the orbital and spin angular momentum are displayed in Figs. 4 and 5, respectively. The orbital angular momentum density always points in the direction of  $-\hat{\theta}l$ , whereas the spin angular momentum density changes its

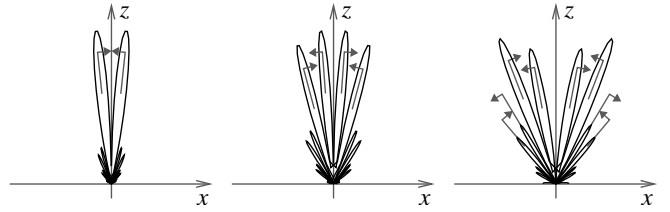


FIG. 5: Radiation patterns for the spin angular momentum. The directions of the spin angular momentum density vectors alternate between  $-\hat{\theta}h$  and  $+\hat{\theta}h$  as displayed by the arrows  $\hat{r}$  and  $\hat{\imath}$ . The patterns are for positive helicity,  $h = +1$ , and topological charge  $l = 0$  (left),  $l = \pm 1$  (middle), and  $l = \pm 2$  (right).

sign from cone to cone. Hence, the directions of the spin angular momentum density vectors alternate between  $-\hat{\theta}h$  and  $+\hat{\theta}h$ .

Often, spin is identified with polarization. We emphasize that this is not allowed for the spin angular momentum *density*; only the total spin angular momentum can be identified with polarization. For instance, taking  $l = 0$  and  $h = 1$ , the spin angular momentum density vanishes on the  $z$  axis, see Fig. 5 (left), whereas the electric and magnetic fields are maximal on the  $z$  axis and are right-hand circular polarized.

## VII. FLUXES

The total fluxes of energy, linear momentum, orbital, and spin angular momentum follow from integrating the densities. Let  $S$  be a closed surface with the antenna array inside it. The total fluxes through the surface are

$$\frac{dF}{dt} = \int_S f c r^2 d\Omega, \quad (39)$$

where  $F$  stands for the total flux  $W$ ,  $\mathbf{P}$ ,  $\mathbf{L}$ , or  $\mathbf{S}$  and  $f$  for the corresponding density  $u_{\text{far}}$ ,  $\mathbf{p}_{\text{far}}$ ,  $\mathbf{l}_{\text{far}}$ , or  $\mathbf{s}_{\text{far}}$ , respectively. Because of the rotational symmetry around the  $z$  axis, the orbital and spin angular momenta,  $\mathbf{L}$  and  $\mathbf{S}$ , are both parallel to the  $z$  axis. The linear momentum is radiated symmetrically in the positive and negative  $z$  directions. Thus, the net vanishes,

$$\mathbf{P} = \mathbf{0}, \quad (40)$$

and the angular momentum of our electromagnetic beams becomes an intrinsic but non-local property.

Expressing the orbital and spin angular momentum in multiples of the total energy, we obtain [2, 30]

$$\frac{L_z}{W} = \frac{dL_z/dt}{dW/dt} = \frac{l}{\omega} \quad (41)$$

and

$$\frac{S_z}{W} = \frac{dS_z/dt}{dW/dt} = \frac{h}{\omega}. \quad (42)$$

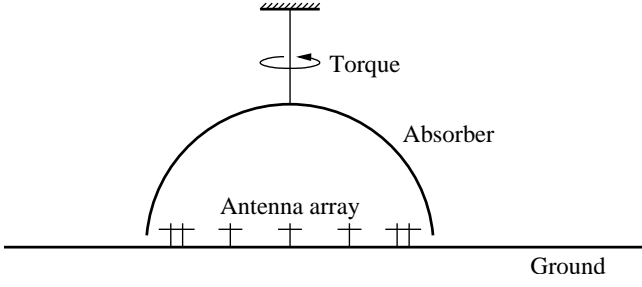


FIG. 6: A radio experiment that measures the torque of the total angular momentum flux.

### VIII. DETECTING THE TORQUE

The torque of the angular momentum flux can, at least in principle, be directly measured with an absorber that surrounds the antenna array in the upper half space; see Fig. 6. If the antenna array is near ground with reflectivity  $\rho_g = I_{\text{refl}}/I_{\text{in}}$ , and if the absorber has a reflectivity of  $\rho_a$  and a transmittance of  $T_a = I_{\text{trans}}/I_{\text{in}}$ , the torque is

$$\frac{d(L_z + S_z)}{dt} = \alpha \frac{l+h}{\omega} \frac{dW}{dt}, \quad (43)$$

where  $dW/dt$  is the power that is radiated by the antenna array and  $\alpha$  is determined by the reflectivities and the transmittance

$$\alpha = \frac{1 + \rho_g}{2} (1 - T_a - \rho_a) \frac{1}{1 - \rho_a}. \quad (44)$$

### IX. RADIO WAVES ASSOCIATED WITH LONGITUDINAL CURRENTS

Based on an idea put forward by Carozzi [37], let us replace the transverse crossed dipoles of the circular antenna array by electric dipoles that point in the longitudinal direction and feed the longitudinal dipole antennas with the currents

$$\mathbf{I}_n = \frac{1}{\sqrt{2}} \begin{pmatrix} 0 \\ 0 \\ 1 \end{pmatrix} e^{2\pi i l \frac{\phi}{N}}, \quad n = 1 \dots N. \quad (45)$$

Then the vector potential reads

$$\mathbf{A} = \frac{1}{\sqrt{2}} \begin{pmatrix} 0 \\ 0 \\ 1 \end{pmatrix} \mathcal{A}(r) \mathcal{C}(\theta, \phi), \quad (46)$$

where  $\mathcal{A}$  and  $\mathcal{C}$  are as given in Section II.

Evaluating the densities of energy, linear momentum, and angular momentum, we obtain

$$u_{\text{far}}^1 = \frac{k^2}{4\mu_0} \left( \frac{I\mu_0 d}{8\pi r} \right)^2 (1 - \cos^2 \theta) (\mathcal{C}^* \mathcal{C}), \quad (47)$$

$$\mathbf{p}_{\text{far}}^1 = \frac{\hat{\mathbf{r}} k^2}{4c\mu_0} \left( \frac{I\mu_0 d}{8\pi r} \right)^2 (1 - \cos^2 \theta) (\mathcal{C}^* \mathcal{C}), \quad (48)$$

and

$$\mathbf{j}_{\text{far}}^1 = l \frac{-\hat{\boldsymbol{\theta}} k^2}{4\omega\mu_0} \left( \frac{I\mu_0 d}{8\pi r} \right)^2 \left( \frac{1 - \cos^2 \theta}{\sin \theta} \right) (\mathcal{C}^* \mathcal{C}). \quad (49)$$

It is useful to compare these densities with those given in Section IV, Eqs. (30)–(32). The essential difference is in the angular momentum density. For pure longitudinal currents, there is only an orbital part,

$$\mathbf{j}_{\text{far}}^1 = \mathbf{l}_{\text{far}}^1, \quad (50)$$

and the spin part vanishes,

$$\mathbf{s}_{\text{far}}^1 = \mathbf{0}. \quad (51)$$

This shows that electromagnetic waves associated with pure longitudinal currents can carry orbital, but no spin angular momentum; cf. the discussion of longitudinal plasma modes in Ref. 24.

Because of the term  $(1 - \cos^2 \theta)$  the beams of electromagnetic waves associated with longitudinal currents have a deep null along their axis of propagation which gives rise to a doughnut shaped beam profile, even in the absence of any topological charge.

The LOIS radio facility [38, 39], currently under construction in Sweden, is the only device that utilizes 3D vector sensing antennas and is readily able to detect these waves. Other radio telescopes, e.g., LOFAR [40] and SKA [41], can be easily reconfigured to achieve the same capability.

### X. GENERALIZING THE RESULTS

From the previous Sections one might get the impression that the analysis is specific to radio beams emitted by a circular antenna array. However, as we now will show, the analysis is more general and device independent.

Any device or source that generates a current distribution on a circle

$$\mathbf{I}(\rho, \Phi, z) = \frac{1}{2} \frac{N}{2\pi R} \frac{1}{\sqrt{2}} \begin{pmatrix} I \\ ihI \\ 0 \end{pmatrix} e^{il\Phi} \delta(\rho - R) \delta(z), \quad (52)$$

where  $\rho, \Phi$ , and  $z$  are cylindrical coordinates, results in the vector potential

$$\mathbf{A} = \frac{1}{\sqrt{2}} \begin{pmatrix} 1 \\ ih \\ 0 \end{pmatrix} \mathcal{A}(r) \mathcal{C}(\theta, \phi) \quad (53)$$

with

$$\mathcal{C} = \frac{N}{2\pi} \int d\Phi e^{i\Phi} e^{-ikR \sin \theta \cos(\Phi - \phi)} \quad (54)$$

and

$$\mathcal{A} = -\frac{I\mu_0 d}{8\pi} \frac{e^{ikr}}{r}, \quad (55)$$

cf. Eqs. (5)–(8). Hence, for the current distribution given here, the results presented in the previous Sections are valid.

Since the angular dependence of the vector potential can be expressed by its residue, Eq. (9), there is no need for the current distribution on the circle itself. Mathematically speaking, the current distribution can be along any path that encircles the origin, provided that the residue is kept unchanged and that no further vortices contribute. Moreover, the current distribution can be chosen arbitrarily in the  $xy$  plane, provided that the residue is kept unchanged. Even if the residue changes, assuming that Eqs. (10) and (11) remain valid, all results presented in this paper, except Figs. 2–5, will hold.

If the current distribution is not in a plane, but in three-dimensional space, knotted optical vortices appear [42].

## XI. INTERFERENCES BETWEEN WAVES ASSOCIATED WITH TRANSVERSE AND LONGITUDINAL CURRENTS

If the vector potential reads

$$\mathbf{A} = \frac{1}{\sqrt{2}} \begin{pmatrix} \alpha \\ \alpha ih \\ \beta \end{pmatrix} \mathcal{A}(r) \mathcal{C}(\theta, \phi), \quad (56)$$

the densities of energy and momenta are

$$u_{\text{far}} = |\alpha|^2 u_{\text{far}}^{\perp} + |\beta|^2 u_{\text{far}}^{\parallel} - 2|\alpha\beta| u_{\text{far}}^{\text{interf}}, \quad (57)$$

$$\mathbf{p}_{\text{far}} = |\alpha|^2 \mathbf{p}_{\text{far}}^{\perp} + |\beta|^2 \mathbf{p}_{\text{far}}^{\parallel} - 2|\alpha\beta| \mathbf{p}_{\text{far}}^{\text{interf}}, \quad (58)$$

$$\mathbf{l}_{\text{far}} = |\alpha|^2 \mathbf{l}_{\text{far}}^{\perp} + |\beta|^2 \mathbf{l}_{\text{far}}^{\parallel} - 2|\alpha\beta| \mathbf{l}_{\text{far}}^{\text{interf}}, \quad (59)$$

$$\mathbf{s}_{\text{far}} = |\alpha|^2 \mathbf{s}_{\text{far}}^{\perp} + |\beta|^2 \mathbf{s}_{\text{far}}^{\parallel} - 2|\alpha\beta| \mathbf{s}_{\text{far}}^{\text{interf}}. \quad (60)$$

The contributions associated with transverse currents are here denoted with the upper index “ $\perp$ ” and are given in Sections IV and V, Eqs. (30)–(35). The contributions associated with longitudinal currents are given in Section IX, and the contributions due to interferences read

$$u_{\text{far}}^{\text{interf}} = \frac{k^2}{4\mu_0} \left( \frac{I\mu_0 d}{8\pi r} \right)^2 \sin\theta \cos\theta (\mathcal{C}^* \mathcal{C}) \cos(h\phi + \arg\beta^* \alpha), \quad (61)$$

$$\mathbf{p}_{\text{far}}^{\text{interf}} = \frac{\hat{\mathbf{r}} k^2}{4c\mu_0} \left( \frac{I\mu_0 d}{8\pi r} \right)^2 \sin\theta \cos\theta (\mathcal{C}^* \mathcal{C}) \cos(h\phi + \arg\beta^* \alpha), \quad (62)$$

$$\mathbf{l}_{\text{far}}^{\text{interf}} = l \frac{-\hat{\boldsymbol{\theta}} k^2}{4\omega\mu_0} \left( \frac{I\mu_0 d}{8\pi r} \right)^2 \cos\theta (\mathcal{C}^* \mathcal{C}) \cos(h\phi + \arg\beta^* \alpha), \quad (63)$$

and

$$\begin{aligned} \mathbf{s}_{\text{far}}^{\text{interf}} = & h \frac{-\hat{\boldsymbol{\theta}} k^2}{4\omega\mu_0} \left( \frac{I\mu_0 d}{8\pi r} \right)^2 \left\{ -\cos\theta (\mathcal{C}^* \mathcal{C}) \right. \\ & \left. + \frac{1}{2} \sin\theta \frac{\partial}{\partial\theta} (\mathcal{C}^* \mathcal{C}) \right\} \cos(h\phi + \arg\beta^* \alpha) \\ & + \frac{-\hat{\boldsymbol{\phi}} k^2}{4\omega\mu_0} \left( \frac{I\mu_0 d}{8\pi r} \right)^2 (\mathcal{C}^* \mathcal{C}) \sin(h\phi + \arg\beta^* \alpha), \end{aligned} \quad (64)$$

respectively.

If integrated, most of the interferences vanish. This allows to carry over the principle of superposition of electromagnetic waves to their mechanical properties,

$$W = |\alpha|^2 W^{\perp} + |\beta|^2 W^{\parallel}, \quad (65)$$

$$\mathbf{P} = |\alpha|^2 \mathbf{P}^{\perp} + |\beta|^2 \mathbf{P}^{\parallel}, \quad (66)$$

$$L_z = |\alpha|^2 L_z^{\perp} + |\beta|^2 L_z^{\parallel}, \quad (67)$$

$$S_z = |\alpha|^2 S_z^{\perp}, \quad S_z^{\parallel} = 0. \quad (68)$$

However, for certain quantities the interferences do not cancel:

$$L_x^{\text{interf}} \neq 0, \quad L_y^{\text{interf}} \neq 0, \quad S_x^{\text{interf}} \neq 0, \quad S_y^{\text{interf}} \neq 0. \quad (69)$$

The consequences of this is the subject of a forthcoming paper.

## XII. DISCRETE SOURCES AND THE UNCERTAINTY PRINCIPLE

If, as in Section X, the sources are continuous, the analysis is exact in the far field and the number of orbital angular momentum states is unbounded. In contrast, if the sources are discrete, the presented analysis is an approximation. Luckily, the approximation improves very fast with the number of discrete sources, and there is typically no need to worry about the accuracy.

However, for the case that only very few discrete sources are present, or if one is interested in the number of orbital angular momentum states that can be utilized, we propose an alternative approach. Namely, starting from a continuous source distribution the discrete nature of the sources is imposed via a “Pacman” shaped mask that has slits at the appropriate positions. Due to Fourier convolution with the mask, the uncertainty principle enters and gives rise to a distribution in the orbital angular momentum [43, 44]. This distribution has a periodicity of  $N$  and peaks of width proportional to  $1/N$  limiting the number of orbital angular momentum states that can be utilized in a circular array of  $N$  equidistributed discrete sources to

$$\#\{l\} = N - O(1/N), \quad (70)$$

where the implied constant in the last term depends on the noise level and on the details of the discrete sources.

## XIII. CONCLUSIONS

Our analysis of the properties of radio beams emitted by a circular antenna array highlights analytically profound aspects of the beam spin and orbital angular momentum. Namely, how the beams are connected to helicity and vorticity; that the angular momentum of the beams is an intrinsic property; that it is transported all the way out to infinity; that it can be separated into spin and orbital angular momentum; and that spin, unlike its density, can be identified with polarization.

In particular, separating the angular momentum into spin and orbital angular momentum, we find that the density of orbital angular momentum depends on the vorticity only and can be expressed in quite simple terms, whereas the density of spin angular momentum depends on both helicity and vorticity.

The approach via an antenna array illuminates the physics from a new perspective and confirms previous studies of orbital angular momentum of electromagnetic beams [2, 30, 34]. Emerging as a byproduct, but being of interest in its own, is the finding in Section IX.

## Acknowledgments

Our sincerest thanks are due to Dr. Tobia Carozzi for very valuable comments and discussions. Part of the work was supported by the Centre for Dynamical Processes and Structure Formation, Uppsala University, Sweden. B. T. gratefully acknowledges financial support from the Swedish Governmental Agency for Innovation Systems (VINNOVA) and the Swedish Research Council (VR).

- 
- [1] J. H. Poynting, Proc. Roy. Soc. London **A 82**, 560 (1909).
- [2] L. Allen, M. W. Beijersbergen, R. J. C. Spreeuw, and J. P. Woerdman, Phys. Rev. A **45**, 8185 (1992).
- [3] R. A. Beth, Phys. Rev. **50**, 115 (1936).
- [4] V. Garcés-Chávez, M. D. Summers, A. Fernandex-Nieves, G. C. Spalding, G. Cristobal, and K. Dholakia, J. Opt. A: Pure Appl. Opt. **6**, S235 (2004).
- [5] M. Babiker, W. L. Power, and L. Allen, Phys. Rev. Lett. **73**, 1239 (1994).
- [6] M. F. Andersen, C. Ryu, P. Clade, V. Natarajan, A. Vaziri, K. Helmerson, and W. D. Phillips, Phys. Rev. Lett. **97**, 170406(4) (2006).
- [7] S. Franke-Arnold, L. Allen, and M. Padgett, Laser & Photon. Rev. **2**, 299 (2008).
- [8] C. N. Cohen-Tannoudji, Rev. Mod. Phys. **70**, 707 (1998).
- [9] K. Ladavac and D. G. Grier, Opt. Express **12**, 1144 (2004).
- [10] M. Harwit, Astrophys. J. **597**, 1266 (2003).
- [11] G. Anzolin, F. Tamburini, A. Bianchini, G. Umbricco, and C. Barbieri, Astron. Astrophys. **488**, 1159 (2008).
- [12] G. A. Swartzlander, Jr., E. L. Ford, R. S. Abdul-Malik, L. M. Close, M. A. Peters, D. M. Palacios, and D. W. Wilson, Opt. Express **16**, 10200 (2008).
- [13] N. M. Elias, II, Astron. Astrophys. **492**, 883 (2008).
- [14] G. Gibson, J. Courtial, M. J. Padgett, M. Vasetsov, V. Pas'ko, S. M. Barnett, and S. Franke-Arnold, Opt. Express **12**, 5448 (2004).
- [15] J. Lin, X.-C. Yuan, S. H. Tao, and R. E. Burge, Appl. Opt. **46**, 4680 (2007).
- [16] A. Mair, A. Vaziri, G. Weihs, and A. Zeilinger, Nature **412**, 313 (2001).
- [17] A. Vaziri, G. Weihs, and A. Zeilinger, J. Opt. B: Quant. Semiclass. Opt. **4**, S47 (2002).
- [18] B. Thidé, H. Then, J. Sjöholm, K. Palmer, J. E. S. Bergman, T. D. Carozzi, Y. N. Istomin, N. H. Ibragimov, and R. Khamitova, Phys. Rev. Lett. **99**, 087701(4) (2007).
- [19] B. Thidé, Plasma Phys. Contr. Fusion **49**, B103 (2007).
- [20] Y. N. Istomin, Phys. Lett. A **299**, 248 (2002).
- [21] B. Thidé, in *Mathematical Modelling of Wave Phenomena*, edited by B. Nilsson and L. Fisherman (Växjö University Press, Växjö, Sweden, 2004), pp. 315–331.
- [22] B. Thidé, E. N. Sergeev, S. M. Grach, T. B. Leyser, and T. D. Carozzi, Phys. Rev. Lett. **95**, 255002(4) (2005).
- [23] M. V. Khotyaintsev, V. N. Mel'nik, B. Thidé, and O. O. Konovalenko, Solar Phys. **234**, 169 (2006).
- [24] J. T. Mendonça, B. Thidé, and H. Then, Phys. Rev. Lett. **in press** (2009), arXiv:0904.2701 [physics.plasm-ph].
- [25] O. Stål, J. Bergman, B. Thidé, L. K. S. Daldorff, and G. Ingelman, Phys. Rev. Lett. **98**, 071103(4) (2007).
- [26] S. Panda, S. Mohanty, J. Padmanabhan, and O. Stål, J. Cosm. Astropart. Phys. **11**, 1 (2007).
- [27] C. Paterson, Phys. Rev. Lett. **94**, 153901(4) (2005).
- [28] L. Norin, T. B. L. Leyser, E. Nordblad, B. Thidé, and M. McCarrick, Phys. Rev. Lett. **102**, 065003(4) (2009).
- [29] T. B. L. Leyser, L. Norin, E. Nordblad, M. McCarrick, T. R. Pedersen, and B. Gustavsson, Phys. Rev. Lett. **102**, 065004(4) (2009).
- [30] S. M. Barnett, J. Opt. B: Quant. Semiclass. Opt. **4**, S7 (2002).
- [31] J. M. Jauch and F. Rohrlich, *The Theory of Photons and Electrons* (Springer-Verlag, Reading, MA, 1980), chap. 2, 2nd ed.
- [32] K. Gottfried, *Quantum Mechanics* (Benjamin, New York, NY, 1966).
- [33] C. Cohen-Tannoudji, J. Dupont-Roc, and G. Grynberg, *Photons and Atoms: Introduction to Quantum Electrodynamics* (Wiley, New York, Chichester, Brisbane, Toronto, Singapore, 1989), chap. 1.
- [34] L. Allen, M. J. Padgett, and M. Babiker, in *Prog. Opt.*, edited by E. Wolf (Elsevier, Amsterdam, Holland, 1999), vol. XXXIX, pp. 291–372.
- [35] L. Josefsson and P. Persson, *Conformal Array Antenna Theory and Design* (John Wiley & Sons, Hoboken, NJ, 2006).
- [36] J. D. Jackson, *Classical Electrodynamics* (Wiley, New York, 1998), 3rd ed.
- [37] T. D. Carozzi, in *7th LOIS Workshop*, edited by B. Thidé (Växjö, Sweden, 2008), URL <http://www.lois-space.net/Workshops/Vaxjo080616-18/Presentations>
- [38] H. Rothkaehl, J. E. S. Bergman, B. Thidé, and Z. Klos, J. Atmos. Sol. Terr. Phys. **70**, 926 (2008).
- [39] LOIS, *LOFAR Outrigger in Scandinavia*, Web site, URL <http://www.lois-space.net>.
- [40] LOFAR, *Low Frequency Array*, Web site, URL <http://www.lofar.org>.
- [41] SKA, *Square Kilometre Array*, Web site, URL <http://www.skatelescope.org>.
- [42] F. Flossmann, K. O'Holleran, M. R. Dennis, and M. J. Padgett, Phys. Rev. Lett. **100**, 203902(4) (2008).
- [43] S. Franke-Arnold, S. M. Barnett, E. Yao, J. Leach, J. Courtial, and M. Padgett, New J. Phys. **6**, 1 (2004).
- [44] J. Řeháček, Z. Bouchal, R. Čelechovský, Z. Hradil, and L. L. Sánchez-Soto, Phys. Rev. A **77**, 032110(13) (2008).